Supporting Information

Martinière et al. 10.1073/pnas.1202040109

SI Materials and Methods

Constructs and Cloning Procedures. ***Fusion of 35s Full-length protein-GFP fusions.*** All genes tested were from *Arabidopsis*. For generating GFP-AGP4, cDNA of AtAGP4 [*Arabidopsis* Biological Resource Center (ABRC) clone number U12380] was used as the PCR template. The signal peptide of AtAGP4 was removed by amplifying the fragment between amino acids 66–704. This DNA was fused by chimeric PCR to the C terminus of sp-mGFP5. The GFP-AGP4 fragment then was inserted into pVKH18En6 using XbaI-SacI restriction sites. cDNA of AtGPA1 (ABRC clone number U12585) and GFP-NPSN11 (1) were used as templates to amplify ORFs of GPA1 and NPSN11, which then were cloned into pENTR/D-TOPO (Invitrogen). pB7WGF2 and pB7FWG2 Gateway (Invitrogen) binary vectors were used to generate GPA1-GFP and GFP-NPSN11 by LR reaction. The other full-length protein fusions with fluorescent protein included At3g17840-GFP and At1g14870-GFP (2), GFP-LTI6b (3), AtFH1-GFP (4), PIP2;1-CFP (5), YFP-SYP121 (1), and GFP-StREM1;3 (6).

Construction of 35s minimal fluorescent proteins. To produce MAP-GFP, the first 36 aa of AtGPA1 were amplified and fused to the N terminus of EGFP by chimeric PCR and were cloned into pBIB using BamHI and SacI restriction sites. For GFP-PAP, nucleotides 243–297 of AtAGG1 (ABRC clone number U82084) were fused to the C terminus of EGFP and were cloned into pBIB using BamHI and SacI restriction sites. For GFP-GPI, the sporamin signal peptide and mGFP5 were amplified from GFP-HDEL and fused to nucleotides 318–405 of AtAGP4. The generated fragment was transformed into pVKH18En6 using XbaI and SacI restriction sites. Other minimal fluorescent proteins (FPs) included GFP-TM23 (7), and YFP-PHFAPP1 [called "YFP-PI" in this study (8)].

Arabidopsis **Stable Transformation and Tobacco Transient Transformation.** Stably transformed *Arabidopsis thaliana* lines used include p35S::PIP2;1-GFP (9), p35S::GFP-LTI6b (2), pUBQ10::YFP-NPSN12 (10), pFLS2::FLS2-GFP (11), p35s::paGFP-LTI6b (12), and pPIN2::PIN2-GFP (13). To transform minimal FP constructs stably, *A. thaliana* cv. Columbia plants were transformed using floral-dip transformation (14). Homozygous T_3 seedlings expressing MAP-GFP, GFP-PAP, GFP-GPI, and YFP-PI were used for the analysis. For GFP-TM23, we used T_1 plants. *Nicotiana tabacum* cv. Petit Havana plants were grown and used in transient transformation experiments as described by Sparkes et al. (15).

Drug Treatments, Cell-Wall Labeling, and Plasmolysis Experiments. *A. thaliana* seedlings were immersed in 25 μM latrunculin B (Calbiochem) (60 min) to remove the actin cytoskeleton, 20 μM oryzalin (Dow Elanco) (60 min) to remove microtubules, or 100 μM filipin III (Sigma-Aldrich) (30 min) to disrupt sterol in the plasma membrane. In protoplast experiments (see below), primary cell-wall regeneration was monitored by staining with 1 μg/mL of Calcofluor White M2R (Sigma-Aldrich). For plasmolysis assays, tobacco leaf sections (approx. 0.25 cm^2) were incubated in a hypertonic solution of 0.5 M mannitol for 30 min and then were mounted in this solution for microscopy. In single molecule tracking experiments, some seedlings were immersed in 20 μM isoxaben (Sigma-Aldrich) for 1 h prior to observation.

Fluorescence Recovery After Photobleaching Experiments. The relative mobile fraction at time 60 s post bleaching (I60s) and relative diffusion rate (D_r) of different FPs was assessed by fluorescence recovery after photobleaching (FRAP) following the technique of Martinière et al. (4) (Fig. S1). Five scans of the entire field of view were made to establish the prebleach intensity of the FP, and then a circular region of interest (ROI) of approximately 57 μm^2 (radius 4.3 μm) was bleached in a median optical section of the fluorescent plasma membrane. Recovery of fluorescence was recorded during 60 or 120 s with a delay of 1.5 s between frames. We confirmed that the energy of the laser used to record postbleach data had no bleaching effect by recording a control region outside the bleaching ROI. Fluorescence intensity data were normalized using the equation:

$$I_n = [(I_t - I_{min})/(I_{max} - I_{min})] \times 100$$

where I_n is the normalized intensity, I_t is the intensity at any time t, I_{min} is the minimum postphotobleaching intensity, and I_{max} is the mean intensity before photobleaching.

Nonlinear regression was used to model the normalized FRAP data. In this case, a two-phase exponential association equation was used:

$$Y_t = A + B\left(1 + \exp^{(-K1)(t)}\right) + C\left(1 - \exp^{(-K2)(t)}\right)$$

where Y_t is normalized intensity, A, B, C, K_1, and K_2 are parameters of the curve, and t is time.

For each treatment, 10–20 cells were analyzed. The value of the fluorescence intensity recovery plateau was calculated for $t = 60$ and was used as an approximation of the relative mobile fraction (I60s).

Values of D_r and I60s were compared using two-tailed t tests or ANOVA followed by Tukey's Honestly Significant Difference (HSD) test using Microsoft Excel and SPSS software.

Total Internal Reflection Fluorescence Microscopy and Single-Molecule Tracking. Total internal reflection fluorescence (TIRF) imaging was performed on a custom-built microscope, equipped with a 100× objective (α-Plan-Fluar, NA = 1.45; Zeiss), 491-nm laser excitation (Cobolt), HQ525/50 nm emission filter (Chroma), and an electron-multiplication CCD (iXon; Andor) (16). Five-day-old seedlings were mounted in a drop of 1/2 strength Murashige and Skoog plant growth medium, pH 5.7, between a slide and a #0 coverslip. The angle of incidence of the excitation beam is continuously adjustable to optimize image contrast. Images were integrated for 30 ms.

Cells overexpressing nonphotoactivated paGFP-LTI6b have a population of naturally fluorescent paGFP molecules that is at a suitable density for TIRF microscopy and single-particle tracking. Plasma membranes were imaged for 30 s at 30 ms per frame.

A Bayesian segmentation-based feature-detection algorithm (17) was used to analyze single-molecule images of paGFP-LTI6b. Spots exhibited the blinking behavior typical for single molecules. Tracks were calculated as described by Rolfe et al. (18). Briefly, features are linked between frames into tracks according to connection probabilities that consider both spatial and temporal proximity, thus allowing tracks of blinking features to be determined. We measured 939 spots in six repetitions. Mean time of plasma membrane (PM) residence and track length were recorded. The mean squared displacement (MSD) was calculated for all molecules:

$$MSD(\Delta t) = \left\langle |r_i(t + \Delta t) - r_i(t)|^2 \right\rangle$$

where $|r_i(t + \Delta t) - r_i(t)|$ is the distance traveled by molecule i between time t and time $t + \Delta t$, and the expectation value is over all pairs of time points separated by Δt in each molecular track.

Detergent-Insoluble Membrane Purification and Western Blot Analysis. Membrane fractionation was done following the protocol of Laloi et al. (18). *A. thaliana* seedlings were homogenized in the presence of 10 mM KH_2PO_4 (pH 8.2) with 0.5M sorbitol, 5% (wt/vol) polyvinylpyrrolidone 40 (Sigma-Aldrich), 0.5% (wt/vol) BSA, 2 mM salicylhydroxamic acid (Sigma-Aldrich), and 1 mM PMSF (Sigma-Aldrich). Homogenates were subjected to successive centrifugations at 1,000 × *g* for 10 min, 10,000 × *g* for 10 min, and 150,000 × *g* for 60 min. Microsomal pellets were suspended in 25 mM Hepes buffer with 3 mM EDTA and 150 mM NaCl (pH 7.4). Microsomal membranes were incubated with 1% Triton X-100 (Sigma-Aldrich) for 30 min at 4 °C (detergent-to-protein ratio of 3) and then were mixed with an equal volume of 72% sucrose (wt/vol), transferred to centrifuge tubes, and overlaid with 40%, 35%, and 30% sucrose solutions. Sucrose gradients were centrifuged 16 h at 190,000 × g_{max}, and eight 500-μL fractions were recovered. Detergent-insoluble membranes (DIM) were found in the top 3 fractions of the gradients. Proteins of each fraction were separated by SDS/PAGE on 12% polyacrylamide gels. Bands were blotted on PVDF membranes (Biorad). For immunolabeling with an anti-GFP (Abcam), PVDF membranes were incubated sequentially with a saturated solution of PBS (1% BSA) for 1 h, with anti-GFP IgGs (Millipore) (1/4,000) for 2 h, and then with the anti–IgG-peroxidase conjugate (Biorad) (1/10,000) for 30 min.

Protoplast Preparation and Immunofluorescence. Tobacco leaf pieces were incubated for 15 h in a solution containing 0.4 M mannitol, 1% cellulase (Sigma-Aldrich) R10, 0.1% macerozyme (Sigma-Aldrich), 1 mM $CaCl_2$, 20 mM KCl, and 10 mM MES at pH 5.6. Protoplasts were used directly for imaging or were labeled for immunofluorescence. Rabbit anti-GFP IgG (1/5,000 dilution) (Abcam), which also detects YFP, and anti-rabbit Texas Red (1/1,000 dilution) (Molecular Probes) were incubated sequentially for 1 h each with two rinsing steps between antibodies and after the secondary antibody.

Cell-wall regeneration experiments were carried out using *A. thaliana* leaf protoplasts. An aliquot of cells was imaged immediately as a time 0 sample. Protoplasts were left at room temperature in light for imaging after 48 h.

1. Foresti O, daSilva LL, Denecke J (2006) Overexpression of the Arabidopsis syntaxin PEP12/SYP21 inhibits transport from the prevacuolar compartment to the lytic vacuole in vivo. *Plant Cell* 18:2275–2293.
2. Dunkley TP, et al. (2006) Mapping the Arabidopsis organelle proteome. *Proc Natl Acad Sci USA* 103:6518–6523.
3. Kurup S, et al. (2005) Marking cell lineages in living tissues. *Plant J* 42:444–453.
4. Martinière A, Gayral P, Hawes C, Runions J (2011) Building bridges: Formin1 of Arabidopsis forms a connection between the cell wall and the actin cytoskeleton. *Plant J* 66:354–365.
5. Sorieul M, Santoni V, Maurel C, Luu DT (2011) Mechanisms and effects of retention of over-expressed aquaporin AtPIP2;1 in the endoplasmic reticulum. *Traffic* 12:473–482.
6. Raffaele S, et al. (2009) Remorin, a solanaceae protein resident in membrane rafts and plasmodesmata, impairs potato virus X movement. *Plant Cell* 21:1541–1555.
7. Brandizzi F, et al. (2002) The destination for single-pass membrane proteins is influenced markedly by the length of the hydrophobic domain. *Plant Cell* 14: 1077–1092.
8. Vermeer JE, et al. (2009) Imaging phosphatidylinositol 4-phosphate dynamics in living plant cells. *Plant J* 57:356–372.
9. Boursiac Y, et al. (2005) Early effects of salinity on water transport in Arabidopsis roots. Molecular and cellular features of aquaporin expression. *Plant Physiol* 139: 790–805.
10. Geldner N, et al. (2009) Rapid, combinatorial analysis of membrane compartments in intact plants with a multicolor marker set. *Plant J* 59:169–178.
11. Robatzek S, Chinchilla D, Boller T (2006) Ligand-induced endocytosis of the pattern recognition receptor FLS2 in Arabidopsis. *Genes Dev* 20:537–542.
12. Martinière A, et al. (2011) Homeostasis of plasma membrane viscosity in fluctuating temperatures. *New Phytol* 192:328–337.
13. Xu J, Scheres B (2005) Dissection of Arabidopsis ADP-RIBOSYLATION FACTOR 1 function in epidermal cell polarity. *Plant Cell* 17:525–536.
14. Zhang X, Henriques R, Lin SS, Niu QW, Chua NH (2006) Agrobacterium-mediated transformation of Arabidopsis thaliana using the floral dip method. *Nat Protoc* 1: 641–646.
15. Sparkes IA, Runions J, Kearns A, Hawes C (2006) Rapid, transient expression of fluorescent fusion proteins in tobacco plants and generation of stably transformed plants. *Nat Protoc* 1:2019–2025.
16. Clarke DT, et al. (2011) Optics clustered to output unique solutions: A multi-laser facility for combined single molecule and ensemble microscopy. *Review of Scientific Instruments* 82, 093705.
17. Rolfe DJ, et al. (2011) Automated multidimensional single molecule fluorescence microscopy feature detection and tracking. *Eur Biophys J* 40:1167–1186.
18. Laloi M, et al. (2007) Insights into the role of specific lipids in the formation and delivery of lipid microdomains to the plasma membrane of plant cells. *Plant Physiol* 143:461–472.

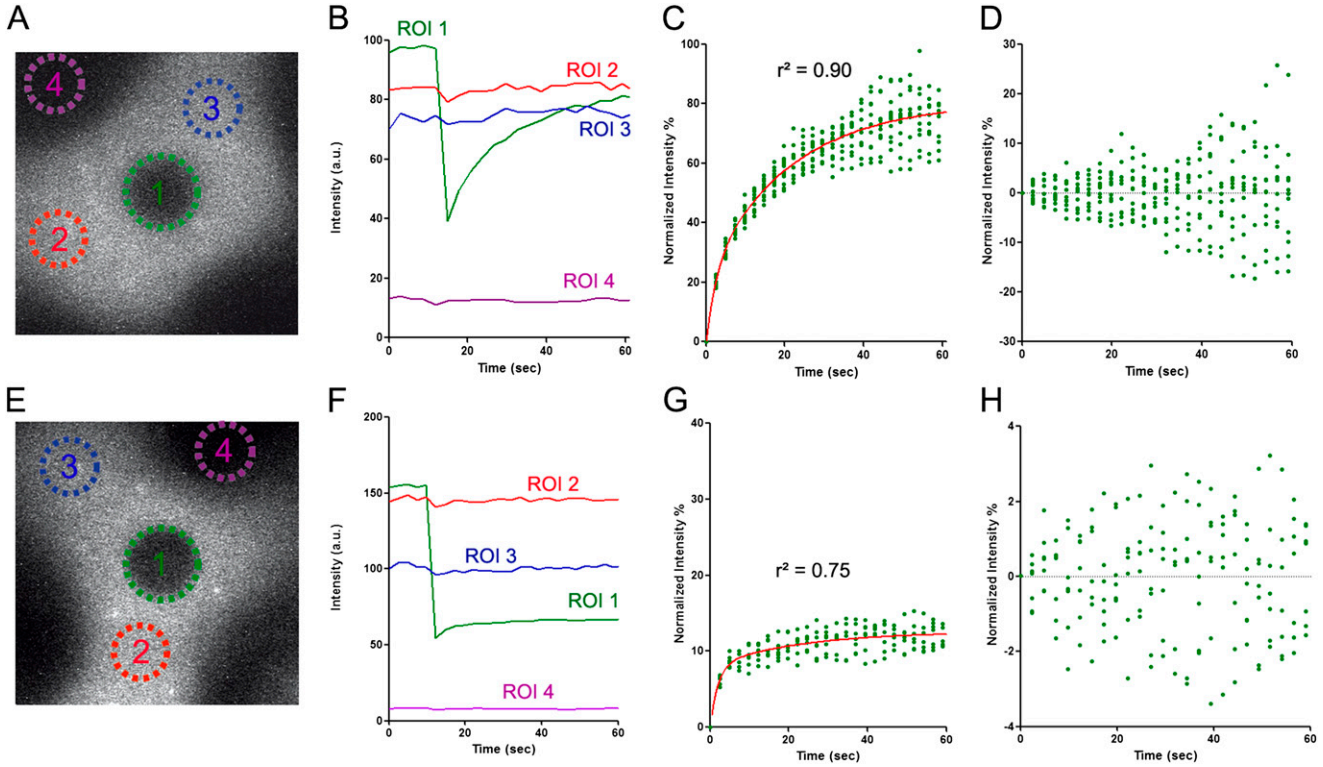

Fig. S1. Detailed analysis of FRAP curves for GPA1-GFP (*A–D*) and GFP-NPSN11 (*E–H*). (*A* and *E*) Analyzed ROI: (1) the bleached spot, (2 and 3) nonbleached plasma membrane regions, and (4) outside the cell. (*B* and *F*) Mean normalized pixel intensities during prebleach and 60-s postbleach recovery phases. Intensity drops sharply within the bleached region and then recovers quickly in the case of GPA1-GFP (*B*) or slowly in the case of GFP-NSPN11 (*F*). Fluorescence intensity within ROIs 2, 3, and 4 remains constant over time illustrating a lack of photobleaching during data-acquisition scanning. (*C* and *G*) Best-fit two-phase exponential curve to model the normalized data set. (*D* and *H*) Distribution of residuals from curve fitting is random.

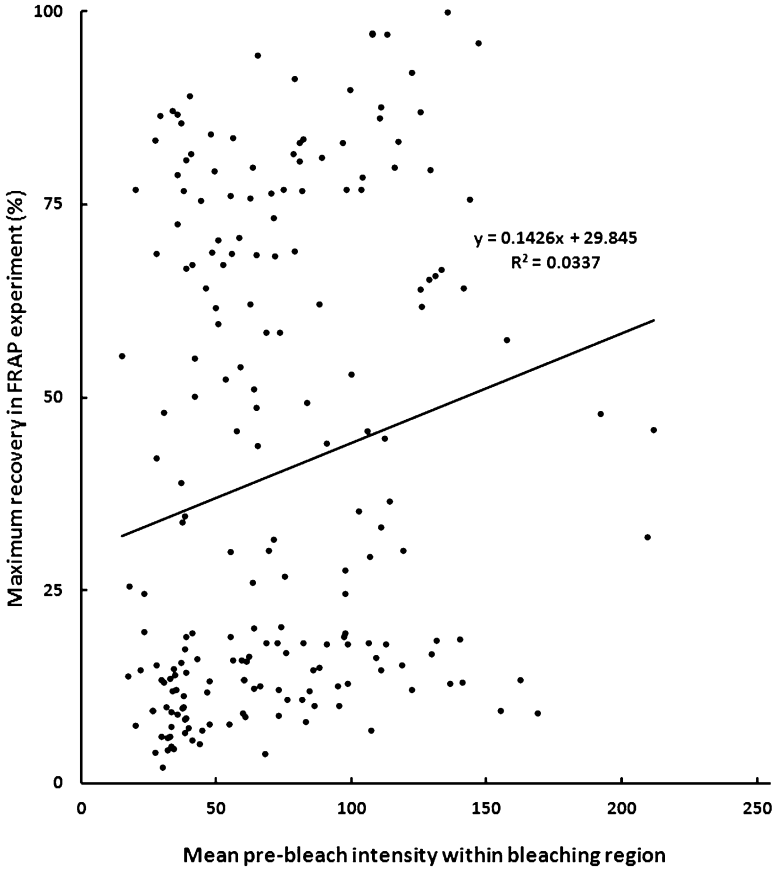

Fig. S2. Mean prebleach intensity within a bleaching region vs. maximum recovery (I60s) during FRAP experiments. No relationship was observed (R^2 = 0.03), suggesting that the amount of protein free to diffuse is independent of the amount of that protein within the PM.

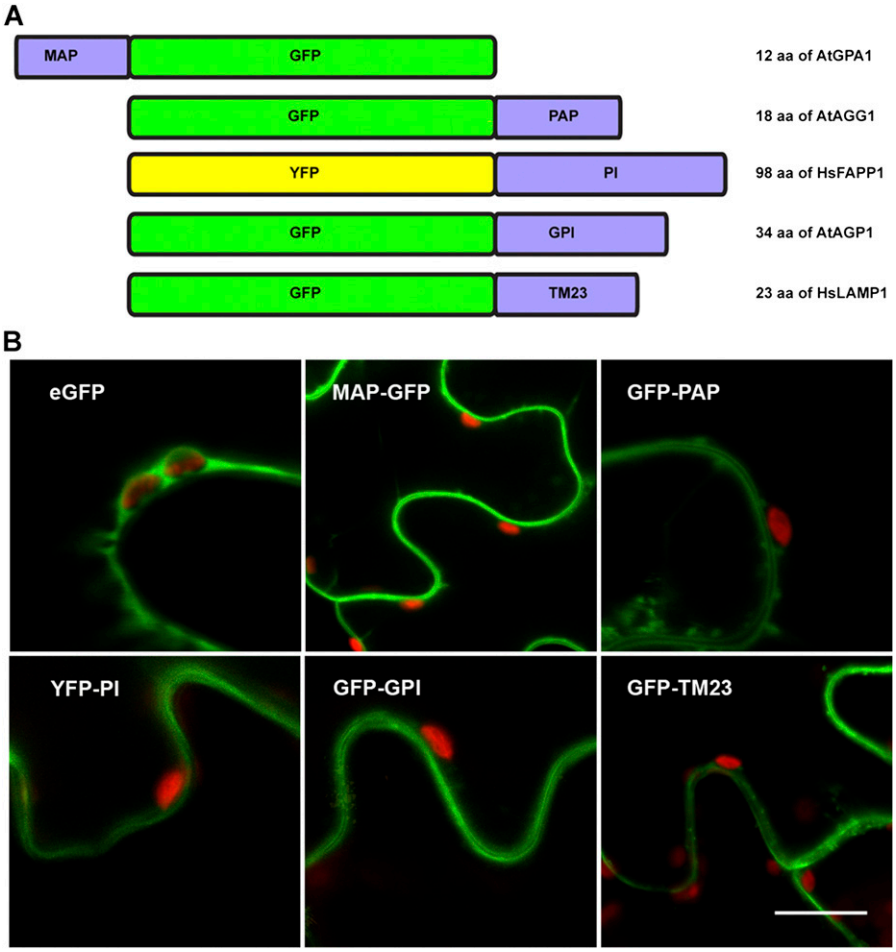

Fig. S3. Minimal FP constructs. (*A*) Schematic of minimal FPs. (*B*) All minimal FPs localized to the PM in tobacco leaf epidermal cells. The GFP signal (green) in cells expressing cytosolic eGFP can be seen surrounding the chloroplasts (red). PM localization means that the GFP always is exterior to chloroplasts for MAP-GFP, GFP-PAP, YFP-PI, GFP-GPI, and GFP-TM23. (Scale bar: 5 μm.)

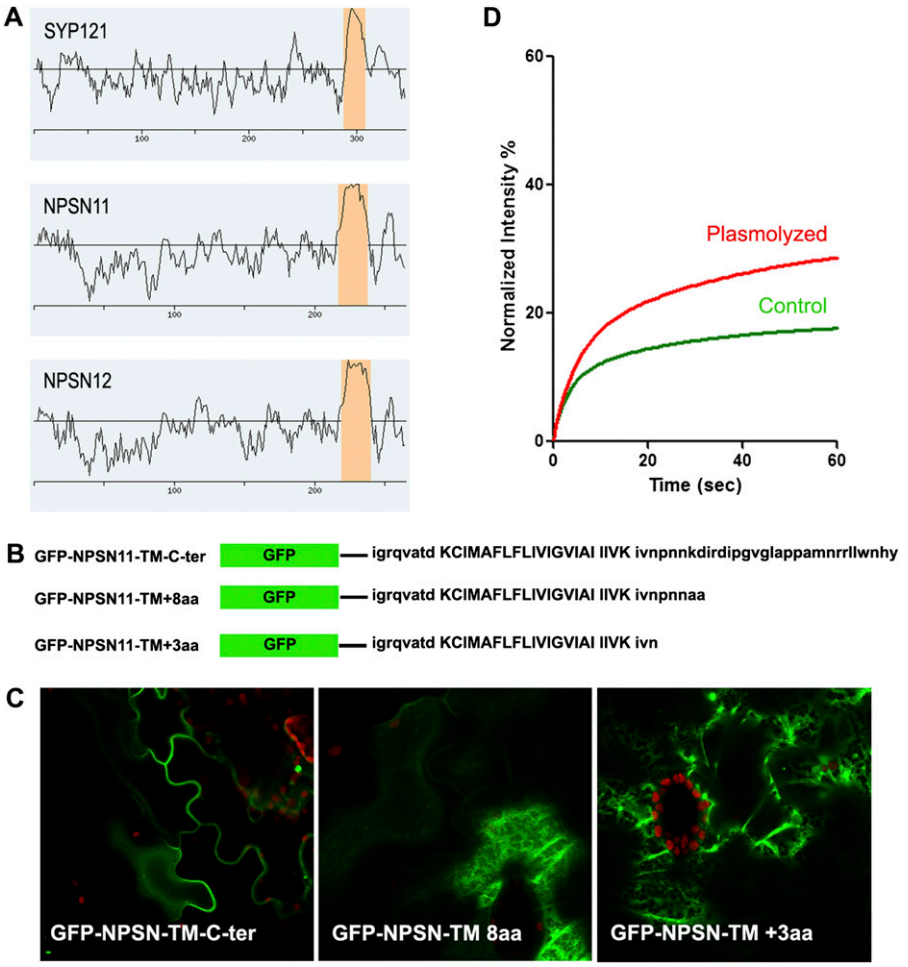

Fig. S4. Attempts to generate a minimal FP construct consisting of an intracellular FP moiety anchored by a single transmembrane domain (TMD). Three soluble NSF attachment protein receptors (SNAREs), SYP121, NSPN11, and NSPN12, were tested as a source of the TMD. (*A*) All three SNAREs were found to possess small extracellular domains as indicated in hydrophobicity plots. The TMD is indicated by shading, and the region to the right of the shading must project into the extracellular space. Plots generated using ARAMEMNON software (1) (http://aramemnon.uni-koeln.de/). (*B*) Three GFP fusions were made with the C-terminal region of NSPN11. The putative TMD is indicated in uppercase. The extracellular domain was shortened successively. (*C*) The putative extracellular tail of NPSN11 is required for proper targeting to the PM. The minimal construct targeted the PM only when the entire C terminus was present. (*D*) FRAP experiments on GFP-NPSN11-TM-C-ter in control and plasmolyzed cells. Deletion of most of the cytoplasmic region of NPSN11 resulted in a small increase in protein mobility (compare with Fig. 1*A*), and plasmolysis increased GFP-NPSN11-TM-C-ter mobility slightly but nonsignificantly.

1. Schwacke R, et al. (2003) ARAMEMNON, a novel database for Arabidopsis integral membrane proteins. *Plant Physiol* 131:16–26.

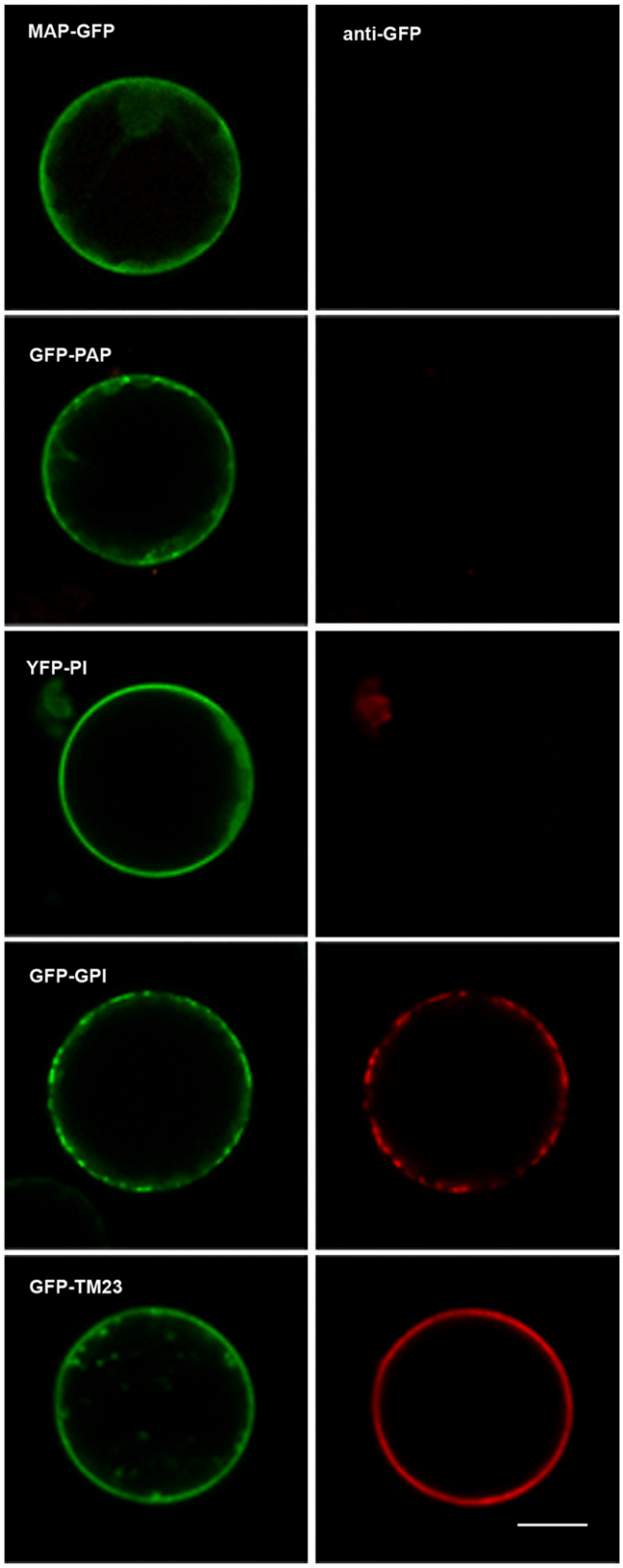

Fig. S5. Immunofluorescence on living tobacco protoplasts expressing minimal FPs. Protoplasts were incubated with an unlabeled rabbit anti-GFP antibody (the antibody also labels YFP; see Fig. S6), which was detected using a goat anti-rabbit antibody coated with Cy5 fluorophore. GFP or YFP (green) marks the PM of all protoplasts, but the PM is labeled by the secondary antibody (red) only when the FP projects into the cell-wall space as for GFP-GPI and GFP-TM23. (Scale bar: 20 μm.)

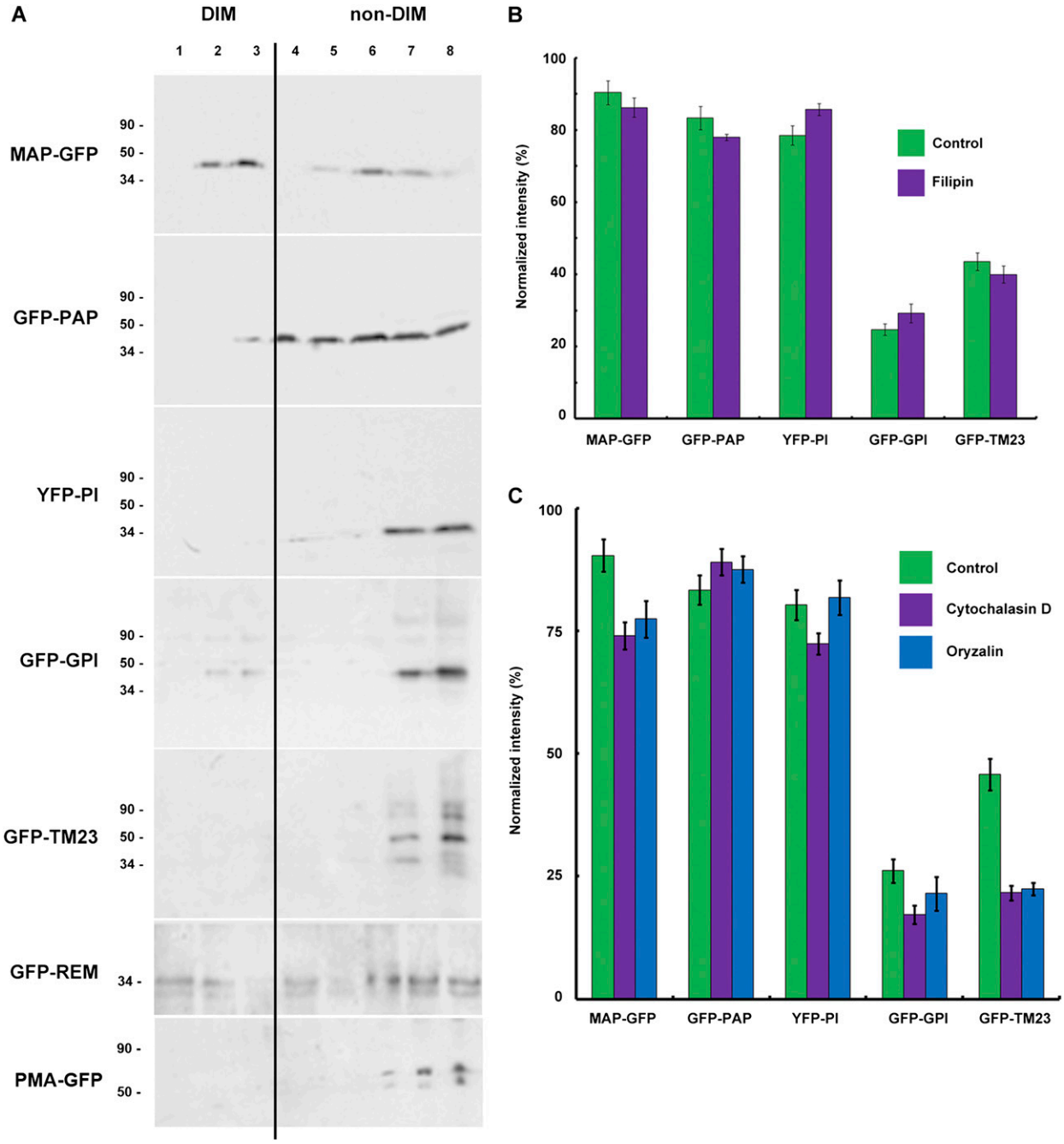

Fig. S6. Lipid domain structure and cytoskeleton have a limited effect on protein mobility in *A. thaliana*. (*A*) DIM fractionation of minimal FP-expressing *A. thaliana* followed by Western blotting with anti-GFP (lanes 1–8 represent position within the fractionation gradient). MAP-GFP and GFP-GPI are present in both DIM and non-DIM fractions, whereas GFP-PAP, YFP-PI, and GFP-TM23 occur primarily in non-DIM fractions. GFP-REM occurs in both DIM and non-DIM fractions, as expected. In contrast, PMA-GFP, a non-DIM protein, is absent from the first five fractions. (*B*) Fluorescence recovery (I60s) of each minimal FP construct in the presence or absence of the sterol-disrupting drug filipin III. Filipin treatment had no effect on protein mobile fraction ($P = 0.87$, two-way ANOVA). (*C*) Fluorescence recovery (I60s) of each minimal FP construct in the presence or absence of cytochalasin D, an actin-depolymerizing drug, or oryzalin, a microtubule-depolymerizing drug. Disruption of cytoskeletons had either no significant effect or induced a decrease in fluorescence recovery (I60s MAP-GFP control vs. MAP-GFP cytochalasin D, $P = 0.003$, Tukey's HSD test; I60s MAP-GFP control vs. MAP-GFP oryzalin, $P = 0.02$, Tukey's test; I60s GFP-TM23 control vs. GFP-TM23 cytochalasin D, $P < 0.001$, Tukey's test; I60s GFP-TM23 control vs. GFP-TM23 oryzalin, $P < 0.001$, Tukey's test).

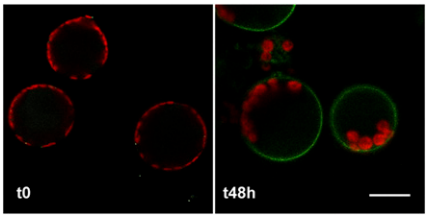

Fig. S7. Cell-wall regeneration in *A. thaliana* protoplasts. Calcofluor white M2R (green) was used to stain cellulose of freshly prepared protoplasts or of cells after 48 h of cell-wall neosynthesis. No cellulose was detectable in freshly prepared protoplasts. Chlorophyll autofluorescence is shown as red. (Scale bar: 10 μm.)

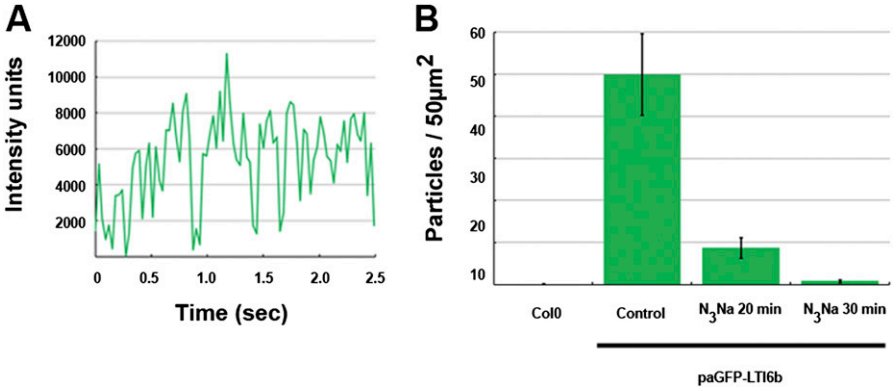

Fig. S8. Single-molecule tracking. (*A*) Fluctuations in intensity of a single molecule during a 2.5-s track. Such blinking is a typical phenomenon for single fluorochrome molecules. (*B*) Quantification of the exocytosis events that mark the appearance of single fluorescent molecules. Nontransformed Col0 cells had virtually no molecules, whereas control cells expressing paGFP-LTI6b had 50 ± 10 molecules per 50 μm^2. Sodium azide treatment, which inhibits exocytosis, significantly reduced the number of molecules.

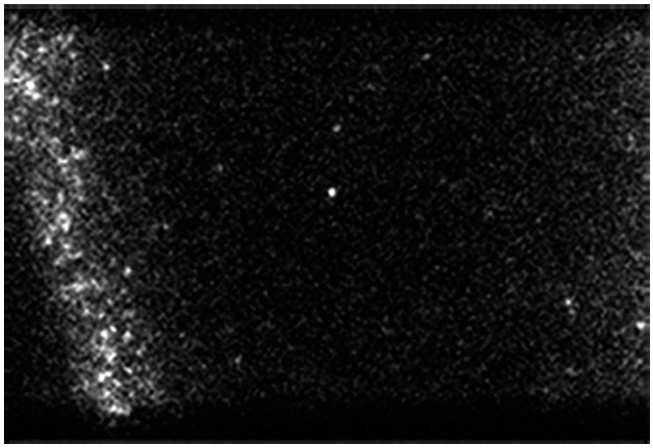

Movie S1. Hypocotyl cells expressing nonphotoactivated paGFP-LTI6b observed using TIRF microscopy with 30-ms time integration and 0.16 μm per pixel. Single particles are visible as short-lived spots brighter than the background.

Movie S1